Gamma-Ray Simulated Spectra Deconvolution of a $LaBr_3$ 1-in. x 1-in. Scintillator for Nondestructive ATR Fuel Burnup Onsite Predictions

Jorge Navarro, Idaho National Laboratory and Center for Space Nuclear Research, 1765 Yellowstone Hwy, P.O. Box, MS 3860, Idaho Falls, ID 83415-3860, jorge.navarro@inl.gov, 208-526-1370

Terry A. Ring, University of Utah, Utah Nuclear Engineering Program/Department of Chemical Engineering, 50 S. Central Campus Dr., Rm. 3290, Salt Lake City, UT 84112-9203

David W. Nigg, Idaho National Laboratory, Reactor Physics Analysis and Design, P.O. Box 1625, MS 3860, Idaho Falls, Idaho 83415-3860

Number of Pages: 34

Number of Figures: 11

Number of Tables: 4

Abstract

A deconvolution methodology aimed to reduce the uncertainty for nondestructively predicting fuel burnup using gamma-spectra collected with $LaBr_3$ scintillators was developed. Deconvolution techniques have been used in the past to improve photo-peak resolution of data collected using gamma detectors; however, they have not been used as a tool to more accurately predict fuel burnup. The deconvolution methodology consisted of calculating the detector response function using Monte Carlo simulations, validating the detector response function against experimental data, and implementing the maximum-likelihood expectation maximization algorithm to enhance the $LaBr_3$ gamma spectra. The deconvolution methodology was first tested on single-isotopic simulated data; later it was applied to fuel-simulated data that were based on Advanced Test Reactor gamma spectra. The study showed that $LaBr_3$ gamma spectra photo-peak resolution and quality can be improved significantly using deconvolution methods, in addition to proving that enhancement techniques can be used to nondestructively predict Advanced Test Reactor fuel burnup more accurately than using $LaBr_3$ data without enhancements.

Keywords: deconvolution, $LaBr_3$, high-enriched fuel burnup prediction

I. Introduction

Collecting data for fuel burnup validation purposes has become a difficult task because capabilities for fuel destructive analysis techniques are being lost, have become difficult to perform, are expensive to implement, and do not allow reuse of the fuel in a new cycle. Existing burnup validation data, in most cases, are outdated and, when data from destructive techniques are available, they are not always representative of the cases that need to be validated or do not account for the entire burnup profile of the fuel. This is especially true for Advanced Test Reactor (ATR) fuel elements, where there is a need to validate the new generation of reactor

physics codes that are being implemented for core management operations. In addition, ATR fuel storage canal operations desire the capability to predict burnup onsite. The necessity for having the capability to collect a gamma spectral data library has been highlighted by the fact that ATR, as well as all reactors operating with highly enriched uranium fuel, will have to convert to low-enriched uranium fuel. Collecting high-quality ATR fuel data will not only be crucial to the computational burnup code validations, it will aid reactor operations personnel in better understanding the behavior of the new low-enriched uranium fuel, especially during the transition period. In addition, because of the imminent conversion of the existing highly enriched uranium research reactors to low-enriched uranium fuel, collecting a library of gamma spectral data before this conversion occurs might represent a unique opportunity for the nuclear community to preserve critical information on highly enriched uranium fuel burnup data.

In response to the clear need to collect validation data on ATR fuel elements for validation of codes and to aid fuel core management operations, a study to determine the feasibility of implementing a system to routinely collect gamma scans from ATR fuel elements was completed during Fiscal Year 2012.1 This project demonstrated that useful gamma spectral data can be collected successfully onsite at the ATR canal. In addition, the feasibility study determined that the collected data could be used as a nondestructive predicting and validation burnup tool. The study tested the capabilities of extracting data using three different detectors: high purity germanium detector, $LaBr_3$, and high pressure xenon detector. After the study completed, it was determined that due to the in-situ nature of the measurements, the $LaBr_3$ scintillators were the best option available to routinely collect fuel data at the ATR canal without affecting canal operations. The $LaBr_3$ scintillators were selected mainly because of their capability to perform under harsh conditions, the possibility of using them for underwater

measurements, low maintenance required, ability to operate at room temperature, and their performance during the study. However, some spectra quality and accuracy, when predicting burnup experimentally using $LaBr_3$, data were lost when compared to the high-purity germanium detector results.

The accuracy and range of operation for nondestructive burnup predictions techniques are highly dependent on the spectra photo-peak resolution. The nondestructive burnup predictions are based on precisely determining the absolute areas or ratio of areas under the peaks of certain isotopes (i.e., $^{134}Cs/^{137}Cs$) and relating them to fuel burnup. However, a shortcoming of the data collected with $LaBr_3$ scintillators during the feasibility study was photo-peak resolution and the impact it had on burnup predictions, isotope identification, and the range of operation over which the predictions were valid.

In order to address this shortcoming, a methodology to enhance the resolution of a $LaBr_3$ 1-in. x 1-in. scintillator was developed. This methodology was aimed at measuring the impact that enhancing photo-peak resolution had on burnup prediction. It has been demonstrated in previous studies that deconvolution can be used for the enhancement of photo-peak resolution in data collected with lower-resolution scintillators[2,3]; however, the application of a deconvolution to $LaBr_3$ scintillators has been limited; in addition, deconvolution previously has not been used to improve the accuracy of nondestructive fuel burnup predictions.

II. $LaBr_3$ 1-in. x 1-in. Scintillator Energy Response Function Determination

The first step in developing an enhancement technique for the permanent system was to determine the detector response function. Successful implementation of a spectrum deconvolution process depends on accurately predicting the detector response as a function of incident gamma-ray energy. The detector response function can be obtained either

experimentally or computationally; both methods are time consuming. The main drawback of the experimental technique is the need for numerous single-peak energy sources and the time that it will take to obtain meaningful counts. The modeling path has three possible options for computing the response function[2]: (1) numerical interpolation, (2) derivation of an empirical analytical function from available experimental response function data, and (3) Monte Carlo simulations.[4,5,6] For this study, the Monte Carlo simulation route was chosen. This route is time consuming; however, it is the method that can provide better accuracy and control of the energy ranges. The Monte Carlo simulation time can be reduced by using a computer cluster. The process of obtaining the response function of the 1-in. x 1-in. $LaBr_3$ scintillator consisted of the following:

- Designing an experiment
- Performing measurements for several gamma radiation sources
- Calculating the Gaussian Energy Broadening parameters needed in MCNPX[7]
- Simulating the experimental setup in MCNPX and validating the model with experimental data collected.

III. Experimental Measurements

Determination of the response function for the $LaBr_3$ detector began by setting up a simple geometry experiment. For this study, the detector was placed on a stainless steel table (Fig. 1) and the source was placed 25 cm from the detector's aluminum entrance window.

The detector used for this study's experiments was a BrilLanCe380 Saint-Gobain detector, which consists of a 1-in. x 1-in. $Labr_3$ scintillation crystal coupled to a photomultiplier tube. The photomultiplier and the scintillator crystal are contained in an aluminum-sealed housing with an aluminum entrance window. Performing experimental measurements to collect

data had two main purposes: (1) to calculate the broadening parameters needed to give the MCNPX simulations Gaussian distribution energy peaks and (2) to validate the Monte Carlo simulation. The counting time of each experimental measurement was 68,400 seconds. Background measurements were taken between single isotope calibration source measurements in order to obtain the net counts for each source. The radioactive sources used in this study are listed in Table I.

IV. Monte Carlo Simulation

The geometrical model of the $LaBr_3$ detector for the experimental measurements was simulated as two concentric aluminum cylinders. The first cylinder represents the sealed photomultiplier chamber's aluminum housing (44.5-cm radius and 114-cm height). The second cylinder simulates the aluminum housing, with an aluminum entrance window (30.4-cm radius and 26.1-cm height), containing the $LaBr_3$ scintillator crystal (25.4-cm radius and 25.4-cm width). In order to have a model that truly represents the interaction between the detectors and the particles measured, the pulse height simulation in MCNPX was given a more realistic Gaussian energy distribution. MCNPX contains a special tally option in which generated parameters from experimental data can be input to the simulation in order to give the spectra the required Gaussian shape.[8] The special tally within MCNPX is called the Gaussian Energy Broadening (GEB) option. The GEB tally gives the detector-simulated data a Gaussian shape by using the unbroadened energy input with the calculated spectral data and user-specified tally inputs to solve Equation 1:[8]

$$f(E) = Ce^{-\left(\frac{E-Eo}{A}\right)^2} \quad (1)$$

where E = broadened energy, Eo = unbroadened energy of the tally, C = normalization constant, and A = Gaussian width, defined by

$$A = \frac{FWHM}{2\sqrt{ln2}} \tag{2}$$

In order to obtain the Gaussian width needed to solve Equation 1, the full width at half maximum (FWHM) of real experimental data is indirectly provided by the user by specifying the three parameters (a, b, and c) in Equation 3 required by the GEB tally

$$FWHM = a + b\sqrt{E + cE^2} \tag{3}$$

The GEB parameters for this particular experimental detection system setup were calculated using the FWHM data acquired from experimental measurements of different gamma sources given in Table II and by performing a nonlinear least square analysis using Matlab. The following are the GEB tally parameters calculated using the experimental measurements needed for MCNPX to give the model spectra Gaussian shaped peaks:

$$\mathrm{a} = 0.0068\ \mathrm{MeV} \quad \mathrm{b} = 0.0058\ \mathrm{MeV}^{1/2} \quad \mathrm{c} = 14.9501\ \mathrm{MeV}^{-1}.$$

Once the simulated spectra had Gaussian pulse height distribution energy-shaped peaks, the next step was to determine if the simulation response function was in good agreement with the experimental gamma-ray source measurements. The validation analysis consisted of comparing the simulated gamma-ray sources (^{60}Co, ^{137}Cs, and ^{226}Ra) spectra against the experimental data collected to determine if there was a good agreement between the two. Figure 2 shows the simulation and experimental spectra of the multi-energy source ^{226}Ra. The plot shows how adding Gaussian energy broadening to the MCNPX pulse height broadening tally allows for an accurate representation of the system's physics. The plot shows that the MCNPX pulse height data peaks were broadened to match the experimental data. The plot also shows that there are some discrepancies in the areas below the peaks; however, for this study, because the protocol will only be applied to simulated data, the interest was only in obtaining

GEB parameters that will give the simulation a realistic Gaussian peak shape, not an absolute match with the experimental data.

V. Response Function Calculation

After the GEB parameters were calculated, the pulse height data distribution for various energy intervals for the 1-in. x 1-in. $LaBr_3$ detector was calculated. The determination of the response function matrix based on experimental measurements was determined by modeling 1300 mono-energetic point sources located at 25 cm from the detector tallying surface. The mono-energetic energy sources varied from 0 to 2,600 KeV with a resolution of 2 keV. Each mono-energetic MCNPX simulation was done using 1 x 10^{10} particles. The calculations were performed using the ICESTORM computer cluster at the Idaho National Laboratory; each MCNPX simulation was executed using 32 processors.

VI. Spectral Deconvolution

Spectral deconvolution (or spectral enhancement) is a technique whose objective is obtaining the most information out of a spectrum taken with a detector measurement system. The theory behind this technique is that in scintillation detectors, the photon incident on the detector crystal may lose part of its energy by photoelectric absorption, Compton scattering, or pair production.[3] However, this information is still recorded in the spectra, just not observed at the appropriate energy region. The deconvolution technique improves the energy resolution of the spectra by moving the counts from those inappropriate regions to the appropriate photo-peaks.[3]

Deconvolution is a powerful technique and, when done correctly, it enhances spectral resolution, allowing for poor-resolution detectors to perform tasks that otherwise would only be suitable for high-resolution detectors. The unfolding process also is very time-consuming and prone to errors. The deconvolution process is highly dependent on the accuracy of the response

function. In addition, the response function's calculations are extremely geometry-sensitive; therefore, every time a different configuration is introduced, a new response function has to be calculated.

Deconvolution of a gamma spectrum can be described in a general manner without reference to any particular experimental system.3 Equation 4 describes the physical process of recording the pulse height data distribution by a detector as the convolution of the true gamma ray spectrum emitted by a source and the response function of the detector

$$\mathrm{M(E)} = \int_0^\infty \mathrm{R(\,E, E_o)S(E_o)dE_o} \tag{4}$$

where $M(E)$ is the measured spectrum, $R(E, E_o)$ is the pulse height data distribution for various energy intervals (response function), and $S(E)$ is the incident spectrum (actual gamma ray spectrum emitted by a radioactive source).

VII. $LaBr_3$ Spectra Deconvolution of Single-Isotopic and Fuel-Simulated Sources using the Maximum Likelihood Expectation Maximization Algorithm

The integral representing the spectrum measured, $M(E)$ can be discretized and represented as a matrix in order to be solved numerically

$$M = RS \tag{5}$$

$$\begin{bmatrix} M_1 \\ \cdot \\ \cdot \\ M_i \end{bmatrix} = \begin{bmatrix} R_{11} \cdots \cdots \cdots R_{1j} \\ \vdots \cdots \cdots \cdots \vdots \\ \vdots \cdots \cdots \cdots \vdots \\ R_{i1} \cdots \cdots \cdots R_{ij} \end{bmatrix} \begin{bmatrix} S_1 \\ \cdot \\ \cdot \\ S_j \end{bmatrix} \tag{6}$$

where M_i represents the true detector counts, R_{ij} is the response function of the detector, and S_j represents the discretized incident spectrum. Ideally, Equation 5 can be solved by a simple matrix inversion.

$$S = R^{-1}M \tag{7}$$

However, the response function matrix for most gamma detection applications is usually large, sparse and ill-conditioned. Specifically, for the problem discussed in this paper, it was quickly determined that the directly inverting the matrix was not appropriate for this study, because it would yield spectra with large oscillations as well as negative results. The solution to Equation 3 can be found using least square fitting iterative algorithms (such as GRV_FC33[9] and SAND-II[10]), as well as using the probabilistic maximum entropy method. For this study, the maximum likelihood fitting by expectation maximization (MLEM) was chosen, because it had previously shown success deconvoluting low-resolution scintillator spectra.2 The MLEM technique also removes the possibility of negative count rates calculated with the deconvolution or unfolding method based upon dn/dE (or Edn/dE) described in Chapter 18 of Knoll's Radiation book,[11] when the least squares fit is resolved without imposing artificial constraints on negative count rates. The MLEM algorithm converges to a maximum-likelihood solution and it converges monotonically, which is another advantaged over the conventional least squares described in Knoll's Chapter 18. The result from the MLEM algorithm has been shown to approximate the true value in the Poisson-statistical sense[12]. The final advantage of the MLEM algorithm is that it preserves counts – the total number of counts in the estimated results equals the total number of counts in the actual detector measurement.

MLEM is an iterative algorithm[12] designed to obtain the best estimate of the true measured spectrum (incident spectrum). The method assumes a Poisson distribution for each independent variable, where M_j is the measured spectrum by the gamma detector and R_{ji} is the response function of the detection system. In this algorithm, it is assumed that ${x_k}^{(n)}$ is the best estimate of the of the actual gamma ray spectrum.[12] The complete derivation of the method can be found in Shepp and Viadi.[13]

$$x_k{}^{(n+1)} = x_k{}^{(n)} \left\{ \frac{1}{\sum_{i=1}^{i} R_{ik}} \sum_{i=1}^{j} \left[\frac{M_i}{\sum_{j=1}^{j} R_{ij}\, x_j^{(n)}} R_{ik} \right] \right\} \tag{8}$$

The algorithm calculates a new value for $x_i{}^{(n+1)}$ in each iteration and it continues until a predetermined tolerance value is reached. The tolerance value is calculated using the mean squared difference between consecutive iterations

$$\mathrm{Tol} = \sum_1^{\mathrm{j}} \left(\mathrm{x}_{\mathrm{j+1}}^{(\mathrm{n})} - \mathrm{x}_{\mathrm{j}}^{(\mathrm{n})} \right)^2 \tag{9}$$

VIII. One Isotope Simulated Sources

The MLEM algorithm described above was implemented in MATLAB and was tested using simulated, one-isotope data created within MCNPX. The data were modeled based on the experimental setup discussed in the previous section, where each isotopic source was modeled in MCNPX with 1 x 10^{10} particles. The results for one peak source ^{137}Cs, double peak source ^{60}Co, and multiple peaks source ^{226}Ra are presented in Fig. 3, 4, and 5, respectively.

In the three istotopic sources' (^{137}Cs, ^{60}Co, and ^{226}Ra) MLEM spectra comparison plots it can be seen that the Compton scattering region and the backscatter peak counts were successfully moved to the appropriate Gaussian shape photo-peaks. In order to further quantify the efficiency of the MLEM deconvolution, the peak-to-total ratio, in conjunction with the energy resolution for the ^{137}Cs and ^{60}Co simulated sources, were calculated. In addition to the energy resolution for the ^{226}Ra its two major photo-peaks were calculated. The results for all measured parameters of one-isotopic sources are presented in Table II.

The numerical results in Table II confirm that the energy resolution improves by a factor of at least 3:1 for each one of the photo-peaks measured for the three one-isotope sources. The

table also shows a significant improvement for the deconvoluted spectra parameter peak-to-total ratios for the three simulated sources.

IX. Fuel-Simulated Sources Deconvolution

Once the MLEM deconvolution algorithm was implemented and tested for the one-isotope simulated sources, a fuel surrogate -source was simulated in MCNPX. The source model was developed because the ATR fuel data collected during the study could not be directly used to calculate the response function of the 1-in. x 1-in. $LaBr_3$ detector for the particular geometrical setup. There is a need to test the performance of the MLEM method for more complicated burnup spectra. The actual experimental detection system used in the study was a temporary setup positioned using a crane and ropes. The experimental setup used during the study did not have the capability of measuring the distance between the system and target (fuel) or the angle of the detection system in regards to the fuel. Consequently, knowing the dimensions of the detection system with any degree of accuracy in order to create an exact MCNPX model for the calculation of the detector response function was not feasible. The response function calculation for deconvolution of spectra using MCNPX needs a precise representation of the experimental setup in order for the model to accurately simulate the interaction of particles with the system collimator, detector, and surroundings. In addition, access to the ATR fuel canal is restricted; therefore, collecting new data to test the deconvolution technique is a difficult task at this time.

The simulated fuel source was developed by first calculating the area of the individual isotope photo-peaks (A_{pp}) from ATR spectra. The second step in obtaining the normalized weighted fuel point source was to calculate the summation of the individual isotope photo-peaks

areas (A_{pp}) from the ATR fuel spectra in order to estimate the total weighted fuel source area (W_{ts})

$$W_{ts} = \sum_{n=1}^{n} A_{pp_n} \tag{10}$$

Once the total weighted fuel source area was calculated, the individual area photo-peaks (A_{pp}) were divided by the result of the total weighted fuel source area (W_{ts}) to obtain the individual isotope concentration (W_{pp}) in the fuel that was used to simulate the surrogate source in MCNPX

$$W_{pp_n} = \frac{A_{pp_n}}{W_{ts}} \tag{11}$$

The method described above was used to create MCNPX spectral data for four individual fuel isotope-weighted point sources representing different ATR fuel element spectra. The MCNPX simulated fuel spectra model was based on the same geometrical setup that was described in the experimental section.

Following the method described, four simulated-point weighted fuel sources were created based on 92% ^{235}U enriched ATR fuel spectra taken at the canal in 2010 as part of a study dedicated to collect burnup validation data[1] (see bottom of Fig. 6). The ATR fuel spectra data were collected as part of a feasibility study to gather data from the ATR canal adjacent to the reactor. The energy intensity and isotopic composition of the simulated point source information was extracted from ATR fuel spectra with different burnup and cooling times.

The comparison of fuel spectral data collected at the ATR canal and the weighted simulated data can be seen in Fig. 6. The figure shows the comparison of simulated and experimental data for element XA374T. The figure also demonstrates that the simulated weighted source was able to reproduce the isotopic peaks of interest in the measured spectra. The

purpose of creating fuel-simulated data during the study was not to have the same exact experiment setup as the ATR detection feasibility study;[1] the objective of simulating highly enriched ATR fuel spectra was to create data to test the MLEM algorithm impact on photo-peak resolution and standard deviation of the burnup calibration curve. There are some discrepancies between the simulated and measured spectra as expected. The differences can be attributed to the fact that the fuel simulation data did not capture the full effects of the original ATR canal experimental setup (i.e., background, minor peaks, or x-ray region). However, the simulated data were able to capture the peaks of interest needed to perform burnup calibrations and will help determine if deconvolution can aid in the prediction of fuel burnup using these calibration methods.

Once the simulated ATR fuel source was proven to be a good representation of the experimental fuel source, the deconvolution algorithm was applied. Figure 7 shows the convoluted spectra of the surrogate ATR fuel element XA569T, while Fig. 8 illustrates the fuel element spectra after deconvolution. Comparing the two figures, it can be seen that the MLEM deconvolution algorithm was effective in moving the losses of energy in the convoluted data to the appropriate photo-peaks in the deconvoluted results. The deconvoluted plot also shows that the MLEM method was efficient in resolving two pairs of close-lying peaks (i.e., 662, 696 and 1332, 1274). This also proves that deconvolution by MLEM helps resolve peaks that have a low number of counts and are lost due to pile-up or lost in the continuum. The better resolution of near-lying peaks and the increase of photo-peak area in small count peaks allows for a better identification of all isotopes present in the simulated fuel source.

In order to test the performance of the MLEM algorithm, four different surrogate element sources, representing four different ATR fuel elements, were modeled with MCNPX. The four

surrogate fuel source spectra were deconvoluted and the energy resolution for the peaks of interest (i.e., ^{134}Cs and ^{137}Cs) was calculated. Table III shows how the energy resolution for ^{134}Cs and ^{137}Cs improves with deconvolution for all the surrogate ATR fuel element sources. Improving the photo-peak energy resolution of the interested peaks means that there will be less fluctuation from pulses recorded at the same energy, yielding less area uncertainty for burnup calibrations.

X. Use of Deconvolution Spectra for Burnup Determination

Development of a deconvolution protocol for ATR fuel burnup prediction is aimed to improve the performance of the nondestructive burnup prediction technique for ATR fuels using robust scintillators. The deconvolution technique is designed to improve spectra quality. Improving the quality of the spectra will, in theory, allow for more confident predictions and a broader range of operation of the 1-in. x 1-in. $LaBr_3$ scintillator for burnup calibrations and other ATR experimental canal applications. Prediction of experimental fuel burnup by fuel calibrations is a technique in which certain peak ratios or peak areas of fission products from gamma-ray spectra are used to nondestructively determine burnup. Figure 9 shows an example of a burnup calibration created with experimental data collected at the ATR canal using an $LaBr_3$ scintillator. The calibration was created using the $^{137}Cs/^{134}Cs$ area ratio versus the known burnup of several fuel elements.

Figure 9 illustrates how the confidence in predicting burnup by this particular nondestructive method decreases for the elements with less than 200 MWd of burnup. The three elements have a cooling time of less than 100 days. A shorter cooling time for a fuel element means that the spectra are dominated by short-lived fission product isotopes; this makes it difficult to use longer-lived ratios or absolute areas commonly used for the creation of burnup

calibrations (^{137}Cs and ^{134}Cs). Because of the higher standard deviation of the ^{137}Cs/^{134}Cs area ratio of elements with short cooling times (i.e., 0 to 100 days), there is no procedure for the future ATR permanent system to calculate burnup from these elements with confidence. The goal of the deconvoluting simulated fuel data is to prove that standard deviation of the ^{137}Cs/^{134}Cs ratio can be decreased, thereby increasing the confidence in the $LaBr_3$ burnup calibration prediction and increasing the cooling time range in which a calibration curve can be used to predict burnup with a certain degree of accuracy.

In order to test the theory that deconvolution can minimize the error of burnup calibrations, two curves based on the photo-peak area ^{137}Cs/^{134}Cs ratios (Table III) were created. Figures 10 and 11 represent the original four surrogate fuel sources' ^{137}Cs/^{134}Cs ratios for the simulated data before and after deconvolution. Figure 10 represents the ^{137}Cs/^{134}Cs burnup calibration curve before deconvolution, while Fig. 11 contains the burnup calibration after deconvolution.

It can be deduced from Fig. 10 and 11 and from the linear fit parameters' standard deviation in Table IV, as well as looking at the error bars associated with the ^{137}Cs/^{134}Cs ratios, that the calibration plot created with the deconvolution data yields a significantly more confident ATR fuel burnup prediction.

XI. Conclusions

This study established that the response function of a 1-in. x 1-in. $LaBr_3$ detector can be calculated using MCNPX. The results show a significant improvement in the energy resolution for all one-isotope sources and improvement of the performance parameters for ^{137}Cs and ^{60}Co peaks. The results also showed that implementing the MLEM deconvolution algorithm will assist a more precise identification of isotopes for fuel element spectra. In addition, this study

determined that the MLEM deconvolution algorithm can be effective in enhancing the energy of the ^{134}Cs and ^{137}Cs peaks for four ATR fuel high-enriched surrogate simulated sources. The study definitively proves that enhancing the resolution of the ^{134}Cs and ^{137}Cs photo-peaks will help to increase the accuracy of burnup calibrations for ATR fuel using a 1-in. x 1-in. $LaBr_3$ scintillator. In conclusion, this methodology was successfully created to increase energy resolution of a scintillator that can be applied to design an efficient and more rugged fuel scanning detection system for the ATR canal for model validation and onsite predictions of burnup.

XII. Acknowledgments

This work was supported by the U.S. Department of Energy under Battelle Energy Alliance, LLC Contract No. DE-AC07-05ID14517.

References

1 J. NAVARRO, R. ARYAEINEJAD, and D. W. NIGG, "A Feasibility Study to Determine Cooling Time and Burnup of Advanced Test Reactor Fuel Using a Nondestructive Technique and Three Types of Gamma-ray Detectors," *J. of ASTM Int.*, 9, 3 (2012).

2 L. J. MENG and D. RAMSDEN, "An Inter-comparison of Three Spectral-Deconvolution Algorithms for Gamma-ray Spectroscopy," *IEEE Transactions on Nuclear Science*, 47, 4, 1329-1336 (2000).

3 J. E. MONAHAN, "Unfolding Measured Distributions," *Scintillation Spectroscopy of Gamma Radiation,* Shafroth, S. M.; Gordon and Breach Science Publishers Inc. New York, 371-386 (1967).

4 J. Y. ZEBALLOS-CHAVEZ et al., "Response Function of a Germanium Detector to Photon Energies Between 6 and 120 KeV," *Nucl. Instruments and Methods in Physics Research*, 457, 212-219 (2001).

5 H. M. HAKIMABAD et al., "Evaluation the Nonlinear Response Function of a 3 x 3 in NaI Scintillation Detector for PGNAA Applications," *Appl. Radiation and Isotopes*, 65, 918-926 (2007).

6 V. KOVALTCHOUCK and R. MACHRAFI, "MonteCarlo Simulations of response for Gas Filled and Scintillator detectors with MCNPX Code," *Annals of Nucl. Energy* 38, 788-793 (2011).

7 X-5 Monte Carlo Team, *April 2003A general Monte Carlo N-Particle Transport Code, Version 5, Overview and Theory*, 1, 106-107, Los Alamos, NM.

8 D. B. PELOWITZ, *MCNPX A General N- Particle Transport Code,* Version 2.6.0, LA-CP-07-1473, Los Alamos, NM.

9 M. REGINATTO, "The "few-channel" unfolding programs in the UMG Package: MXD_FC33, GRV_FC33 and IQU_FC33," UMG package, Version 3.3 (2004).

10 W. N. MCELROY, S. BERG, T. CROCKETT, and R. G. HAWKINGS, *A computer-automated iterative method for neutron flux spectra determination by foil activation*, U.S. Air Force Weapons Laboratory, AFWL-TR-67-41, Kirkland AFB, NM (1967).

11 G. KNOLL, "Radiation Detection and Measurements," Wiley Third Edition.

12 *Maximum-Likelihood Expectation-Maximization (ML-EM) Iterative Reconstruction Algorithm*, UC Berkley.

13 L. A. SHEPP and Y. VARDI, "Maximum Likelihood Reconstruction for Emission Tomography," *IEEE Trans. Medical Imaging,* 1, 2, 113-122 (1982).

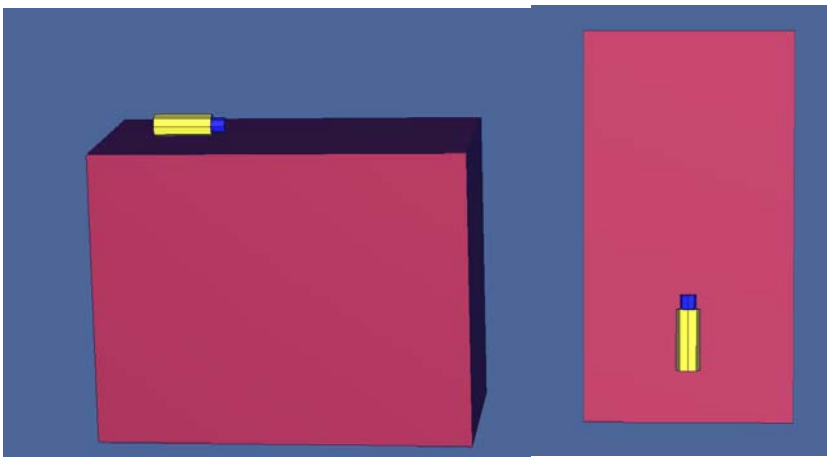

(a) (b)

Fig. 1. MCNPX experimental setup side view (a) and top view (b).

TABLE I Gamma Energy Sources Used for GEB Parameters

Nuclide	Energy (KeV)	FWHM (keV)
Ba K_α X-ray	32.29	8.25
^{152}Eu	121.52	9.23
	244.8	12.88
	344.45	15.39
	778.98	24.8
	867.08	27.47
	964.01	26.96
	1408.01	39.17
^{137}Cs (662 peak)	659.32	22.51

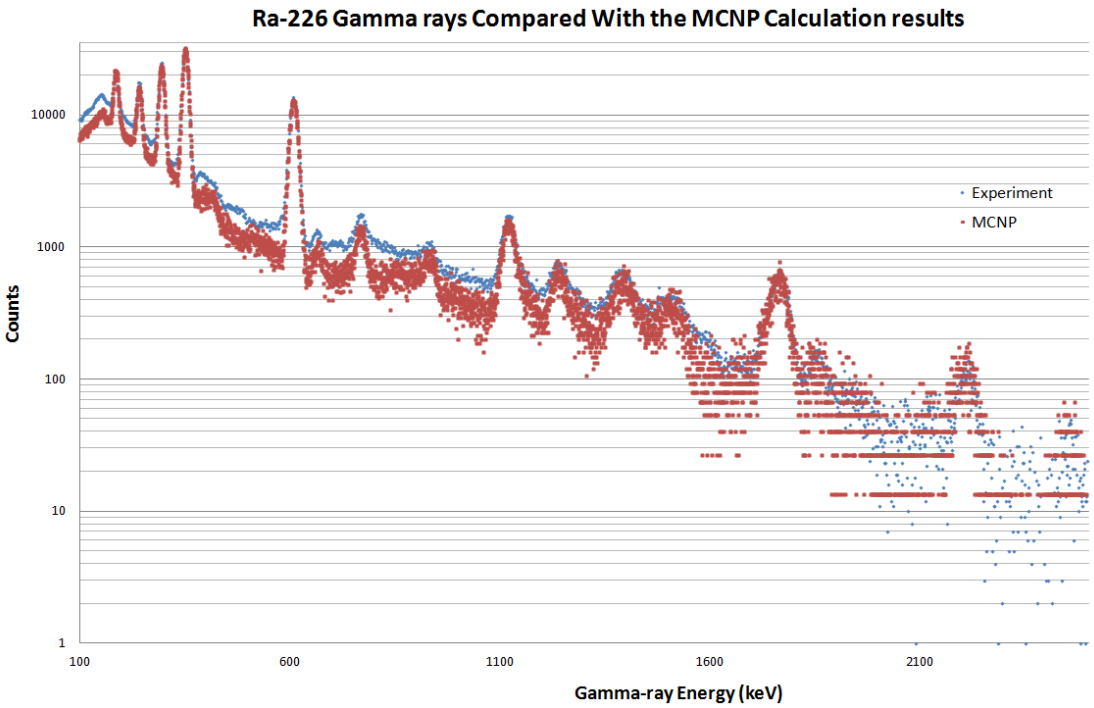

Fig. 2. Ra-226 experimental and simulated MCNP spectra.

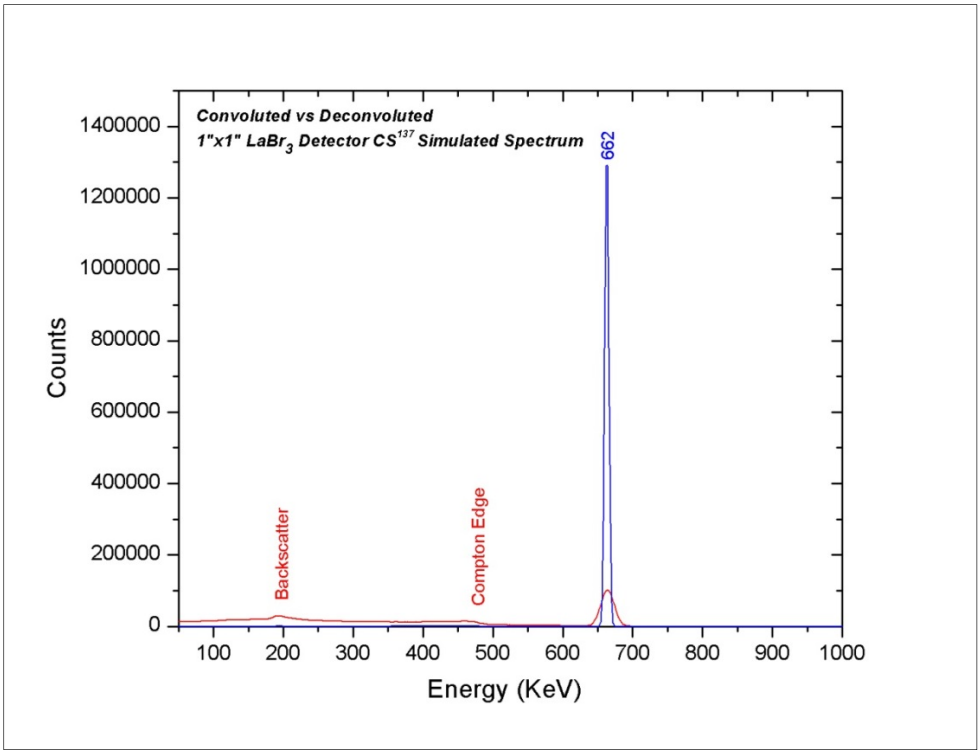

Fig. 3. Simulated convoluted spectrum of a ^{137}Cs source.

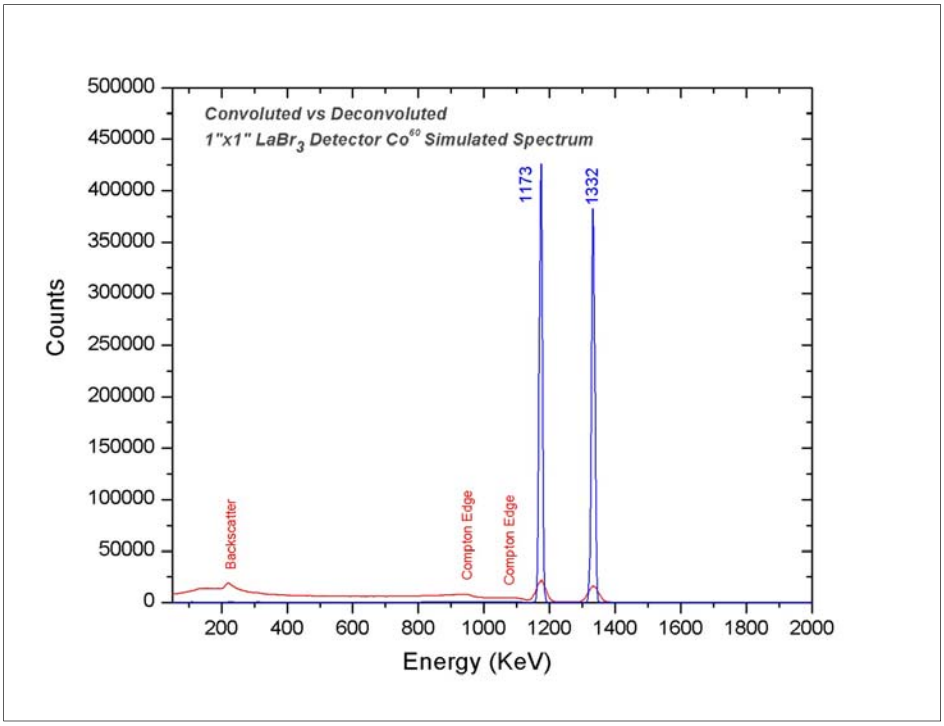

Fig. 4. Simulated convoluted spectrum of a ^{60}Co source.

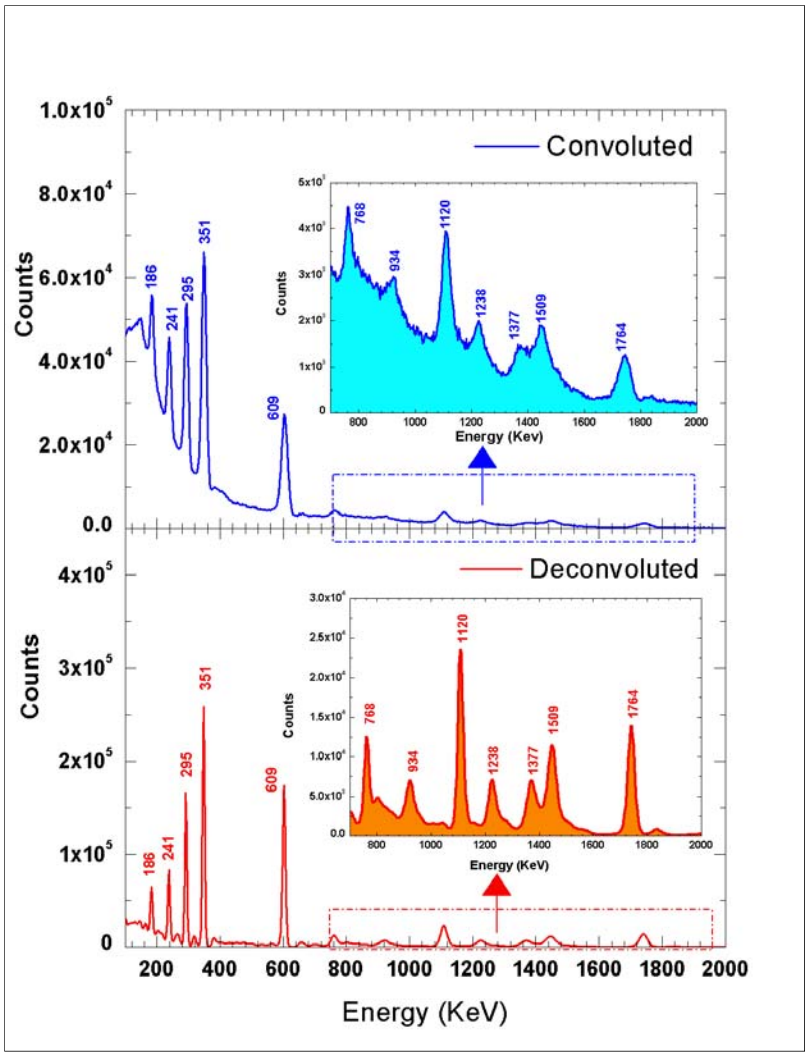

Fig. 5. Simulated spectrum of a ^{226}Ra source.

TABLE II Simulated One Isotope Deconvolution Performance Measurements

Source	Peak Energy (KeV)	Spectrum	Peak Resolution (%)	Peak /Total
^{137}Cs	662	Simulated Spectrum	3.35	0.49
		Simulated Deconvolution	1.05	2.05
^{60}Co	1173	Simulated Spectrum	2.92	0.15
		Simulated Deconvolution	0.92	0.99
	1332	Simulated Spectrum	2.81	0.13
		Simulated Deconvolution	0.87	0.95
^{226}Ra	351	Simulated Spectrum	4.41	0.22
		Simulated Deconvolution	0.98	0.39
	609	Simulated Spectrum	3.45	0.12
		Simulated Deconvolution	1.09	0.48

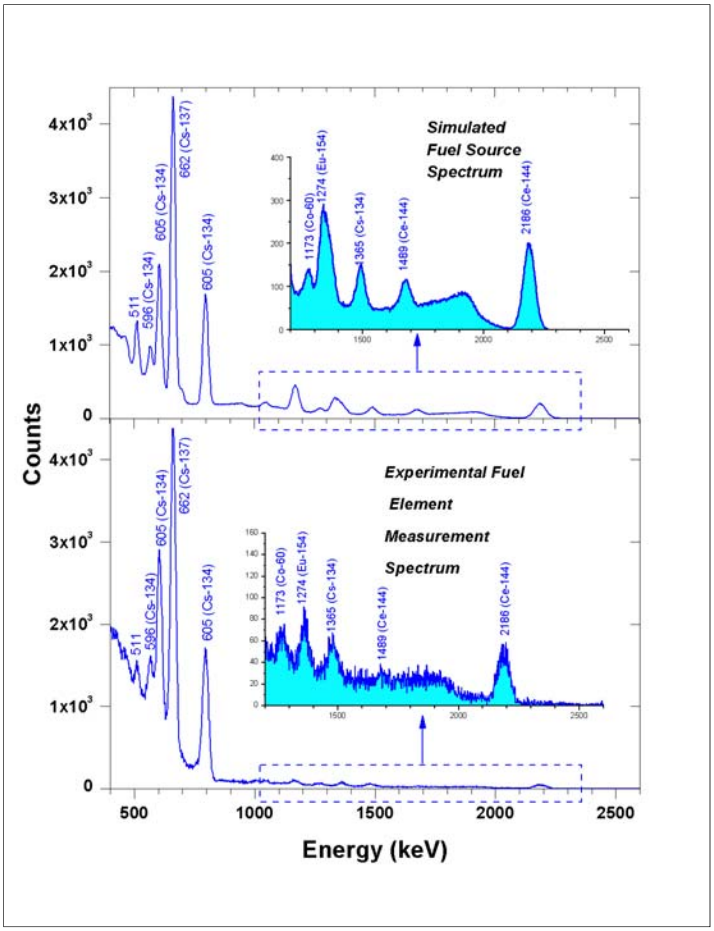

Fig. 6. Experimental and simulated fuel ATR spectra comparison.

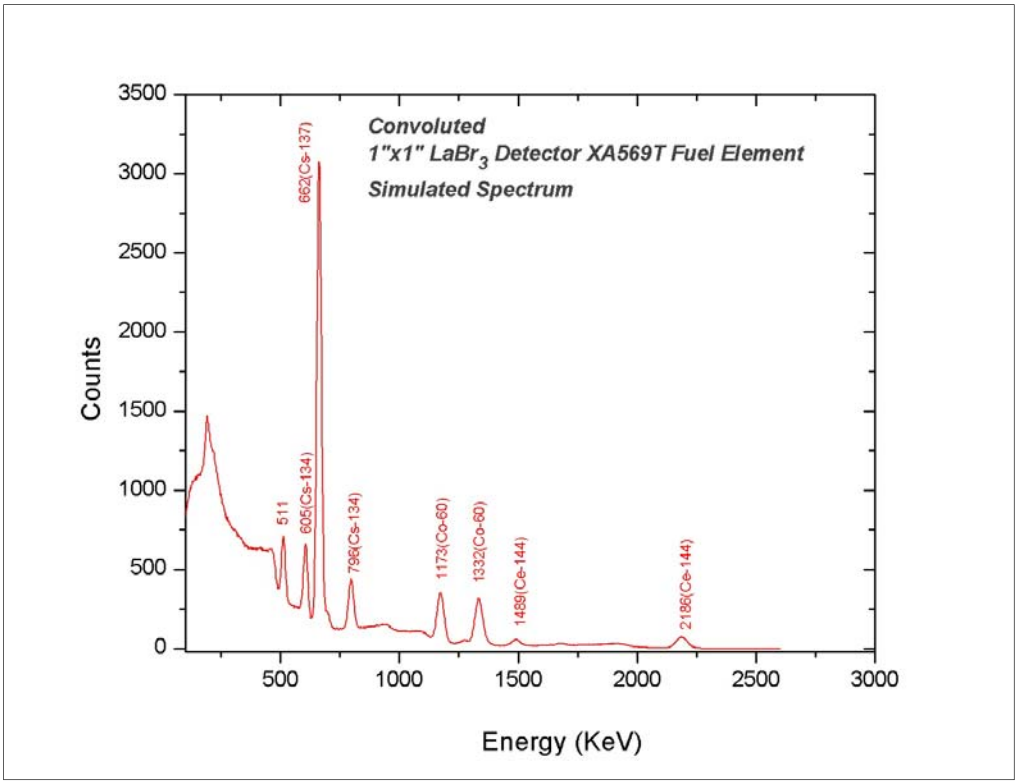

Fig. 7. Convoluted simulated fuel ATR spectra.

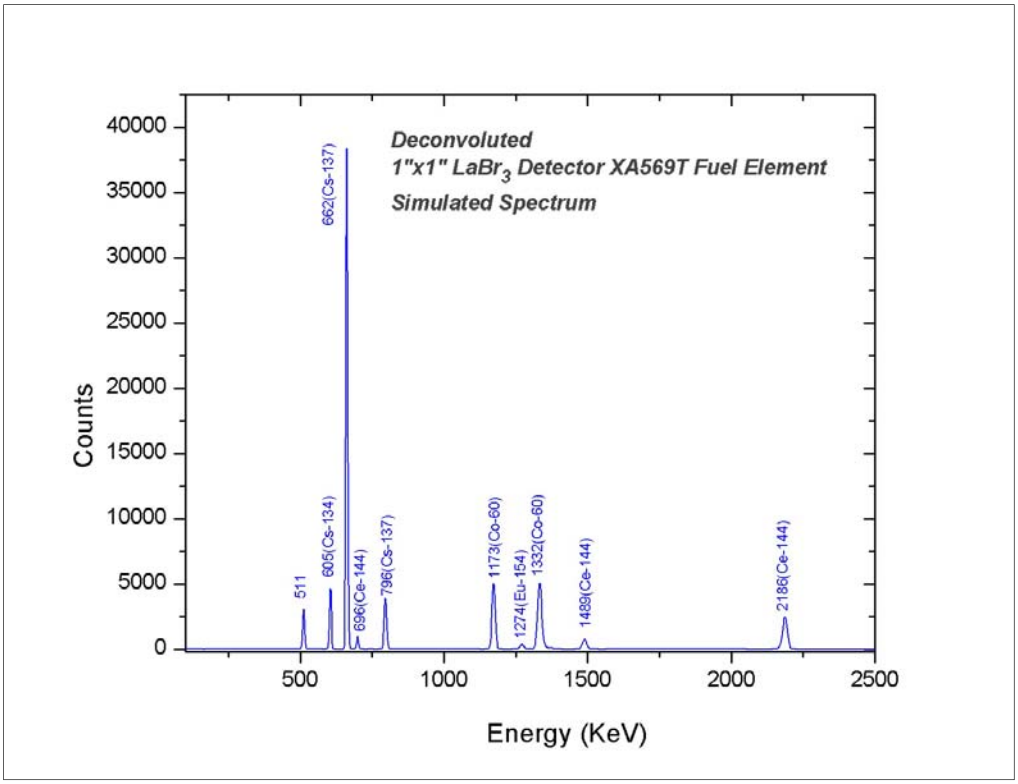

Fig. 8. Deconvoluted simulated fuel ATR spectra.

TABLE III Surrogate Fuel Elements Photo-Peaks Resolution

	Convoluted		Deconvoluted	
Element	**Peak Resolution ^{134}Cs**	**Peak Resolution ^{137}Cs**	**Peak Resolution ^{134}Cs**	**Peak Resolution ^{137}Cs**
Xa569T	3.59	3.36	1.23	1.25
Xa377T	3.58	3.29	1.48	1.18
Xa374T	3.55	3.34	1.24	1.1
Xa379T	3.36	3.28	1.54	1.31

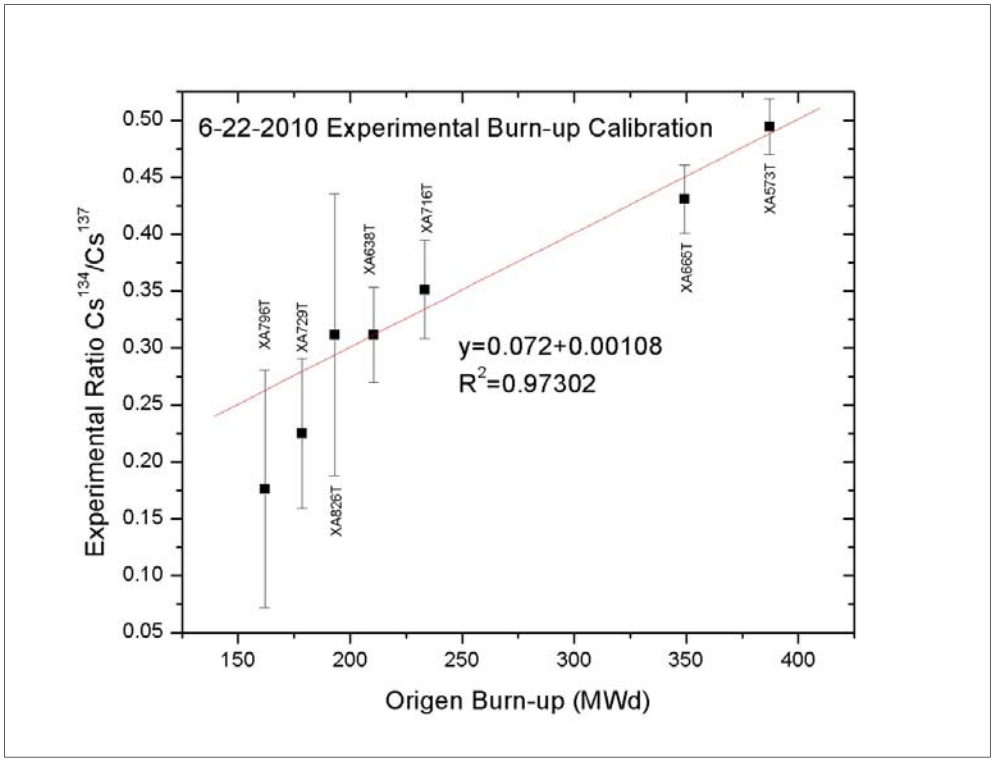

Fig. 9. Example of an ATR fuel burnup prediction calibration.

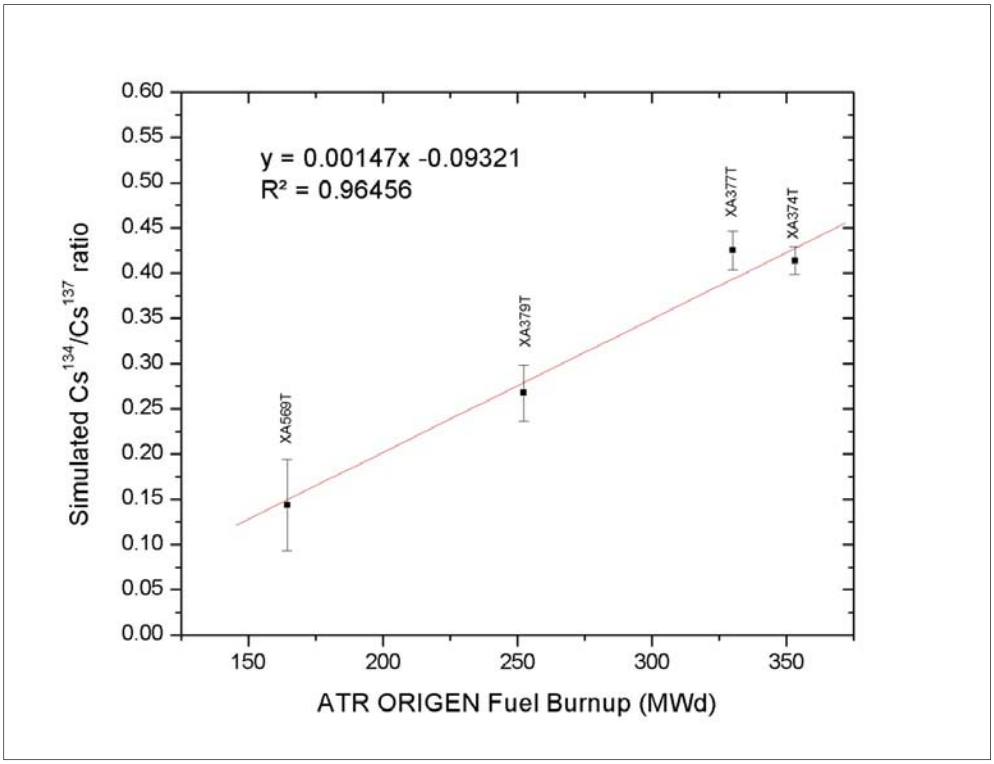

Fig. 10. Convoluted burnup calibration simulated fuel ATR spectra.

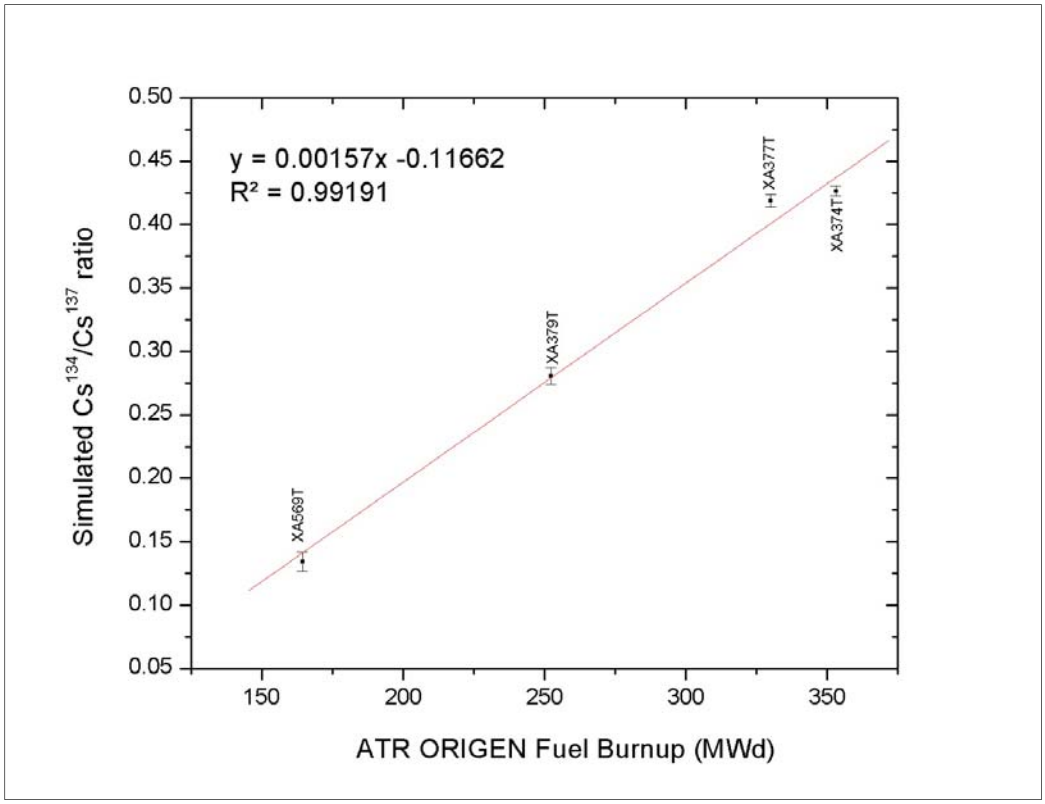

Fig. 11. Deconvoluted burnup calibration simulated fuel ATR spectra.

TABLE IV Linear Fit Parameters Values and Errors (y=mx+b)

Parameter	**Convoluted Value**	**Convoluted Error ±**	**Deconvoluted Value**	**Deconvoluted Error ±**
b	-0.09321	0.0753	-0.11662	0.01322
m	0.00147	2.30E-04	0.00157	4.17E-05